Warming Trends Increasingly Dominate Global Ocean

Gregory C. Johnson[1] and John M. Lyman[1,2]

[1]*NOAA/Pacific Marine Environmental Laboratory, Seattle WA 98115, USA*

[2]*Joint Institute for Marine and Atmospheric Research, University of Hawai'i at Manoa, Honolulu HI 96822, USA*

manuscript for *Nature Climate Change*

11 May 2020

Corresponding author: Gregory C. Johnson (gregory.c.johnson@noaa.gov)

Abstract

The ocean takes up about 93% of the global warming heat entering Earth's climate system. Additionally, the associated thermal expansion contributes substantially to sea level rise. Hence, quantifying the oceanic heat uptake rate and its statistical significance has been a research focus. Here we use gridded ocean heat content maps to examine regional trends in 0–700 m ocean warming from 1993–2019 and 1968–2019, time periods based on sampling distributions. The maps are from four different research groups, three based on ocean temperature alone and one combining ocean temperature with satellite altimeter sea level anomalies. We show that use of longer time periods results in larger percentages of ocean area with statistically significant warming trends, and less ocean area covered by statistically significant cooling trends. We discuss relations of these patterns to climate phenomena including the Pacific Decadal Oscillation, the Atlantic Meridional Overturning Circulation, and global warming.

An ongoing increase of greenhouse gas concentrations in the atmosphere coupled with the long response timescales and large thermal capacity of the oceans and the cryosphere have led to an energy imbalance: Less energy leaves Earth's climate system than enters it. From 1971 to 2010 around 93% of this excess energy went into warming the oceans, with 3% melting ice, 3% warming the land, and only 1% warming and moistening the atmosphere (where the latent heat energy for evaporation to maintain relative humidity is roughly equivalent to the energy to warm the atmosphere)[1]. Furthermore, ocean warming is tightly linked to sea level rise, with expansion owing to that warming accounting for about 42% of global average sea level rise since 1993 (ref.

2). Thus, global depth-integrated ocean temperature change is a key metric of a changing climate[3], with ocean warming tightly linked to increases in atmospheric greenhouse gas concentrations.

The IPCC Fifth Assessment Report estimated the global energy imbalance for 2005–2010, which as noted above is dominated by ocean warming, as equivalent to 0.6 (±0.4) W m^{-2} applied over the entire surface area of Earth (their Fig. 2.11)[1]. Argo measurements since 2010 have greatly narrowed the uncertainty of estimates of ocean heat uptake, so that the global energy imbalance for 2005–2016 has been estimated as 0.7 (±0.1) W m^{-2} in one study[4]. The ocean heat uptake values in that study over the Argo sampling range for similar time periods are in good agreement with those reported in other studies[5,6].

Determining rates of globally integrated ocean heat content is not a trivial task, as ocean temperature measurements have been made with a wide variety of instruments, with varying accuracy, to varying depths, and at varying spatial and temporal resolution[7]. Historical data coverage generally wanes back in time, towards the south, and with increasing depth[3,7,8]. With the advent of the expendable bathythermograph (XBT), the upper 450 m of the ocean began to be sampled widely around 1968, at least in the shipping lanes, i.e., to around 30°S. By about 1993, deep XBTs measuring to 700 m were in common use, largely owing to the efforts of the World Ocean Circulation Experiment. As noted above, the Argo array of profiling floats first reached sparse global coverage in 2005 or 2006, accurately measuring ocean temperatures to nearly 2000 m (ref. 9).

Regional subsurface ocean temperature (as well as subsurface salinity and sea level) distributions also vary substantially with climate phenomena or patterns such as El

Niño[10,11], the Pacific Decadal Oscillation[12,13], the North Atlantic Oscillation[14], and with other large-scale variations in wind stress over the ocean, for instance in the South Pacific[15]. These prominent variations of subsurface ocean temperature associated with large-scale changes in winds and currents, as well as air-sea heat fluxes, over time scales from interannual to multi-decadal, mean that regional ocean temperature (and sea level) trends are often larger and less certain than global integrals of those quantities[16]. Studies of sea level in climate simulations suggest that it can take decades to nearly a century to detect the long-term greenhouse-gas forced signal of sea level locally in the face of these other presumably natural variations, with the detection time dependent on the region[17].

Here we pose intermediate questions regarding ocean warming: What fraction of the upper ocean exhibits a statistically significant warming or cooling trend (without formal attribution) over time periods varying from 5 years (arguably the shortest time period over which one could compute statistical significance of a trend) to the record length? How do the large-scale patterns of variability in upper ocean heat content trends over the record length relate to prominent climate phenomena, both natural and anthropogenic?

To investigate those questions we generate maps of annual 0–700 m ocean heat content anomalies from 1993–2019 by combining sea level anomaly data from satellite altimeters with ocean temperature data[18,19] , hereafter denoted PMEL maps (for NOAA's Pacific Marine Environmental Laboratory) and use 0–700 m annual maps from ocean temperature data from three other research groups, hereafter denoted JMA[20] (for Japan Meteorological Agency, IAP[21] (for Institute of Atmospheric Physics, Chinese Academy of Sciences), and NCEI[22] (for NOAA's National Center for Environmental Information) for analyses spanning the years 1993–2019 and 1968–2019. The selection of these time periods is motivated by improvements in the observational record in 1968 and again in 1993 (ref. 8). The 1993–2019 maps are more robust, but analyzing 1968–2019 provides some useful insights. We then analyze trends from the record lengths (27 and 52 years) down to 5-year intervals, assessing their regional statistical significance.

Ocean warming trends for 1993–2019 PMEL maps are skewed, with 16% of the area occupied by negative trends and 84% by positive trends (Fig. 1a). However, these trends are not everywhere statistically significantly different from zero (see Methods and Data). Limiting the area to statistically significant regions results in 56% of the ocean surface analyzed being covered by significant positive trends, but only 3% of the ocean surface area by significant negative trends (Fig. 1a, black contours; Table 1), even more skewed towards positive values than the analysis without regard to statistical significance. Local values of the 27-year trends range from a minimum of -8 W m^{-2} to a maximum of 7 W m^{-2} for the PMEL maps, much larger than the average trend for the ocean surface area of 0.60 W m^{-2} (equivalent to 0.42 W m^{-2} applied uniformly over Earth's surface). In comparison, trends for 90% of the ocean area analyzed lies between -0.4 and 1.8 W m^{-2}, again skewed towards positive values.

Areas of statistically significant ocean warming trends for 1993–2019 are similarly skewed for the other maps (Fig. 1b–d; Table 1), with the largest skewness for IAP maps (68% positive and 5% negative) and the smallest for NCEI maps (57% positive and 10% negative). Looking at the longer time period of 1968–2019 (Fig. 2) the areas with statistically significant positive trends become even larger, and those with statistically significant negative trends even smaller. Again, for 1968–2019 trends, IAP maps are the most skew (80% positive and 1% negative) and NCEI maps the least (72% positive and 3% negative). There are not PMEL maps for this time period, since satellite altimetry began around 1993, and the PMEL maps incorporate satellite altimetry data.

Calculating the statistically significant areas with positive and negative trends for each of the possible 5-year trend estimates, 6-year trend estimates, and so on to the one possible 27-year (or 52-year) trend estimate, reveals that the longer the time periods used for the trend estimates, the larger the ocean surface area occupied by statistically significant warming, whatever group's maps are used (Fig. 3). We deem 5 years the shortest time period for which statistical significance of a trend might plausibly be estimated. For 1993–2019 (Fig. 3a) the average of the 5-year trend maps (they provide only about 5.4 degrees of freedom because of substantial overlaps in time of successive 5-year periods) with statistically significant warming and cooling areas amounts to 24% and 17%, respectively, for the PMEL (combined) map, with similar values for the other (in situ only) maps. The increases in areas with statistically significant warming trends and decreases in areas with statistically significant cooling trends with longer time periods are monotonic for all the maps. These positive and negative areas are generally statistically distinct with respect to estimates of their 5–95% confidence limits (see Methods and Data for details) for $\geq$ 7-year time periods for all the different products used in the 1993–2019 analysis (Fig. 3a).

While the areas with statistically significant positive and negative 5-year trends are quite similar for the 1993–2019 (Fig. 3a) and 1968–2019 (Fig. 3b) analyses, the latter are statistically distinct even for 5-year trends (Fig. 3b), probably owing to a nearly doubled record length and consequent increase in degrees of freedom. In addition, the variance of the maps before 1993 may be smaller in some data-sparse regions (e.g., south of 30°S), which could be another contributing factor. For a given trend length, the areas with statistically significant positive trends are slightly larger and those with negative trends are slightly smaller for the 1993–2019 analysis than for the 1968–2019 analysis, respectively. This difference (which is well within the uncertainties) is likely owing to a stronger global warming signal in more recent times. However, it could also be owing to decreased data coverage in earlier years, which will generally tend to bias the maps for those years towards the climatological values, potentially reducing warming trends during those times.

The global integral of the local record-length trends for annual 1993–2019 upper (0–700 m) ocean heat content PMEL maps yields a heating rate of 212 TW, equivalent to 0.42 W m^{-2} applied to the entire surface area of Earth (5.10×10^{12} m^2) over the entire 27-year record. This result fits well within confidence limits of trend estimates from six different groups based solely on in situ observations for 0–700 m from 1993–2018, which range from 0.36 (±0.15) to 0.42 (±0.06) W m^{-2} (Ref. 19). This good agreement of the global estimates for the combined altimeter/in situ PMEL maps with in situ-only estimates is reassuring, since determining the precise value of a relatively small residual global average value from a field with much larger regional variations is not trivial.

Both the 1993–2019 (Fig. 1) and the 1968–2019 (Fig. 2) ocean heat content trends from all the research groups yield very consistent large-scale patterns for each time period. However, the trends for the two time periods have somewhat different regional patterns. These patterns are mostly linked to previously reported climate phenomena. We will focus on the better-sampled 1993–2019 trends (Fig. 1). For instance, from 1993 to

2019 there is a pronounced warming associated with each of the subtropical western boundary currents: the Gulf Stream in the North Atlantic, the Brazil Current in the South Atlantic, the Agulhas Current in the South Indian, the Kuroshio in the North Pacific, the East Australia Current in the South Pacific, and to a lesser extent perhaps even the Somali Current in the North Indian Ocean. These areas of stronger warming are consistent with that found in sea-surface temperature analysis, and have been linked to an intensification and poleward shift of the western boundary currents associated with changes in the surface winds[23]. However, the cooling trends equatorward of the Gulf Stream extension, Kuroshio extension, and Agulhas retroflection observed here indicate reductions in the upper ocean baroclinic shear with time in these regions. This pattern has been noted previously for the Gulf Stream extension, and even linked to a possible reduction in the Atlantic Meridional Overturning Circulation (AMOC)[24]. The pattern along the Kuroshio has been studied, and is more complex, but also shows reductions in strength in the downstream region[25].

A pronounced upper ocean warming trend from 1993–2019 in the Southern Hemisphere extends across the South Atlantic, the South Indian, and much of the South Pacific oceans (Fig. 1) and stores much of the ocean's long-term greenhouse gas warming[5,6]. This pattern has been observed both over shorter[5,15] and longer[26,27] time periods (including 1968–2019, see Fig. 2) and is seen in an analysis of climate model projections[28]. It may be largely owing to upwelling of very old waters in the Southern Ocean, their uptake of heat in adjustment to present surface conditions, and subsequent subduction and northward spread into the subtropical gyre[29]. However, its structure has also been linked in part to a spin-up of the subtropical gyres with changes in surface winds[5,15].

In the Pacific Ocean, significant 1993–2019 warming trends are present in the center of the North and South Pacific basins in the vicinities of the western boundary current extensions, and the western tropics (Fig. 1). Weak trends, with small areas of cooling, are present in the eastern tropics, eastern sides of the basins, and high latitudes. This pattern is reminiscent of the Pacific Decadal Oscillation (PDO)[30] in the North Pacific and the Interdecadal Pacific Oscillation (IPO)[31] in both hemispheres. Temperature anomalies in the PDO and IPO, and in the North Pacific have been linked to sea level and circulation changes[13]. The PDO does trend downwards from 1993 to 2019, with a trend fit to index values dropping by 0.45 over that time period. In contrast, the drop is only 0.30 for a trend fit to the PDO from 1968 to 2019, and the PDO pattern in the ocean heat content trends over that time period is not as distinct (Fig. 2) as for the shorter, more recent time period (Fig. 1).

In the tropical Pacific, a rapid rate of increasing sea level (associated with the upper ocean warming) in the western portion of the basin has been associated with increases in trade winds[32], although that pattern reversed over the past few years[33]. While that western Pacific increase is visible in the 1993–2019 trends (Fig. 1) it is not in the 1968–2019 trends (Fig. 2).

The upper Indian Ocean 1993–2019 ocean heat content trends exhibit warming almost throughout for both 1993–2019 (Fig. 1) and 1968–2019 (Fig. 2), again with stronger warming in the Southern Hemisphere. A strong warming trend in sea-surface temperature has been reported previously there, and attributed to both greenhouse gas warming and changes in the character of El Niño in recent decades[34]. The size of the warming trend is substantially smaller for the longer time period, consistent with an increased warming rate in recent decades.

The 1993–2019 trend towards a warmer upper ocean (and higher sea levels) along the east coast of North America and cooling (with lower sea levels) in the subpolar North Atlantic (Fig. 1) is highly reminiscent of a pattern that has been linked to a reduction in the strength of the AMOC in models[35]. Similar trends are visible for the 1968–2019 period, with the subpolar cooling muted over the longer time period. A reduction in AMOC strength starting in 2009, relative to 2004–2008 has also been documented observationally and discussed[36], with 2004 being the first year of AMOC observations with a trans-Atlantic moored array. Our analysis indicates that the changes are large and long-term enough to support a statistically significant pattern in the 1993–2019 trends of upper ocean heat content, and even the 1968–2019 trends. However, the link of the cooling in the subpolar North Atlantic to reductions in the AMOC is difficult to disentangle, with a strong interannual cool event centered around 2015 being caused mostly by strong heat loss from the ocean to the atmosphere, rather than reduced advection of warm water northward associated with an AMOC reduction, which is expected to occur on longer time scales[37].

While the regional variations of upper ocean heat content trends are large, even for all possible 5-year periods in the records, the average total area of the ocean with statistically significant positive trends for all possible 5-year periods from 1993–2019 using the PMEL maps, 24%, is substantially larger than that with statistically negative trends, 17% (Fig. 3). For the 27-year 1993–2019 trend, this difference increases to 53%

of the ocean area with statistically significant positive trends versus 3% of the ocean area with statistically significant negative trends. The PMEL, JMA, IAP, and NCEI maps show similar patterns for 1993–2019 (Fig. 1) and the latter three for 1968–2019 (Fig. 2), with similar statistics for the record length trends (Fig. 3, Table 1). The means, standard deviations, and ratios of their magnitudes computed for the record-length trends from maps of all the research groups show large areas of agreement (Extended Data Fig. 1). The asymmetry for the 1968–2019 record length trends is even more pronounced than for the 1993–2019 trends (Fig. 3, Table 1). For the 52-year 1968–2019 trends, from 72 to 79% of the ocean area has statistically significant positive trends versus the 1 to 3% of the ocean area with statistically significant negative trends. It may take a long time for the long-term global warming signals in upper ocean heat content or sea level[17] to emerge in the face of interannual to multi-decadal variability. Even so, comparisons of observed ocean heat content trends, observed sea level trends, and those from climate models provide valuable insights[38,39]. Moreover, not only does the global average show a clear trend, but for ≥ 7-year trends distinctly (in a statistically significant sense) more of the ocean area shows statistically significant positive trends than shows statistically significant negative trends.

References

1 Climate Change 2013: The Physical Science Basis. *Climate Change 2013: the Physical Science Basis*, 1-1535 (2014).

2 Cazenave, A. *et al.* Global sea-level budget 1993-present. *Earth System Science Data* **10**, 1551-1590, doi:10.5194/essd-10-1551-2018 (2018).

3 Meyssignac, B. *et al.* Measuring Global Ocean Heat Content to Estimate the Earth Energy Imbalance. *Frontiers in Marine Science* **6**, doi:10.3389/fmars.2019.00432 (2019).

4 Johnson, G. C., Lyman, J. M. & Loeb, N. G. CORRESPONDENCE: Improving estimates of Earth's energy imbalance. *Nature Climate Change* **6**, 639-640 (2016).

5 Roemmich, D. *et al.* Unabated planetary warming and its ocean structure since 2006. *Nature Climate Change* **5**, 240-245, doi:10.1038/nclimate2513 (2015).

6 Wijffels, S., Roemmich, D., Monselesan, D., Church, J. & Gilson, J. Ocean temperatures chronicle the ongoing warming of Earth. *Nature Climate Change* **6**, 116-118 (2016).

7 Abraham, J. P. *et al.* A Review of Global Ocean Temperature Observations: Implications for Ocean Heat Content Estimates and Climate Change. *Reviews of Geophysics* **51**, 450-483, doi:10.1002/rog.20022 (2013).

8 Lyman, J. M. & Johnson, G. C. Estimating Global Ocean Heat Content Changes in the Upper 1800 m since 1950 and the Influence of Climatology Choice. *Journal of Climate* **27**, 1945-1957, doi:10.1175/jcli-d-12-00752.1 (2014).

9 Roemmich, D. *et al.* On the Future of Argo: A Global, Full-Depth, Multi-Disciplinary Array. *Frontiers in Marine Science* **6**, doi:10.3389/fmars.2019.00439 (2019).

10 Johnson, G. C. & Birnbaum, A. N. As El Nino builds, Pacific Warm Pool expands, ocean gains more heat. *Geophysical Research Letters* **44**, 438-445, doi:10.1002/2016gl071767 (2017).

11 Roemmich, D. & Gilson, J. The global ocean imprint of ENSO. *Geophysical Research Letters* **38**, doi:10.1029/2011gl047992 (2011).

12 Palanisamy, H., Meyssignac, B., Cazenave, A. & Delcroix, T. Is anthropogenic sea level fingerprint already detectable in the Pacific Ocean? *Environmental Research Letters* **10**, doi:10.1088/1748-9326/10/8/084024 (2015).

13 Wills, R. C. J. *et al.* Ocean Circulation Signatures of North Pacific Decadal Variability. *Geophysical Research Letters* **46**, 1690-1701, doi:10.1029/2018gl080716 (2019).

14 Kenigson, J. S., Han, W. Q., Rajagopalan, B., Yanto & Jasinski, M. Decadal Shift of NAO-Linked Interannual Sea Level Variability along the US Northeast Coast. *Journal of Climate* **31**, 4981-4989, doi:10.1175/jcli-d-17-0403.1 (2018).

15 Roemmich, D., Gilson, J., Sutton, P. & Zilberman, N. Multidecadal Change of the South Pacific Gyre Circulation. *Journal of Physical Oceanography* **46**, 1871-1883, doi:10.1175/jpo-d-15-0237.1 (2016).

16 Carson, M. & Harrison, D. E. Regional Interdecadal Variability in Bias-Corrected Ocean Temperature Data. *Journal of Climate* **23**, 2847-2855, doi:10.1175/2010jcli3121.1 (2010).

17 Richter, K. & Marzeion, B. Earliest local emergence of forced dynamic and steric sea-level trends in climate models. *Environmental Research Letters* **9**, doi:10.1088/1748-9326/9/11/114009 (2014).

18 Willis, J. K., Roemmich, D. & Cornuelle, B. Combining altimetric height with broadscale profile data to estimate steric height, heat storage, subsurface

temperature, and sea-surface temperature variability. *Journal of Geophysical Research-Oceans* **108**, doi:10.1029/2002jc001755 (2003).

19 Johnson, G. C. *et al.* in *State of the Climate in 2019* Vol. 100(9) S74-S77 (Bulletin of the American Meteorological Society, 2019).

20 Ishii, M. *et al.* Accuracy of Global Upper Ocean Heat Content Estimation Expected from Present Observational Data Sets. *Sola* **13**, 163-167, doi:10.2151/sola.2017-030 (2017).

21 Cheng, L. J. *et al.* Improved estimates of ocean heat content from 1960 to 2015. *Science Advances* **3**, 10, doi:10.1126/sciadv.1601545 (2017).

22 Levitus, S. *et al.* World ocean heat content and thermosteric sea level change (0-2000 m), 1955-2010. *Geophysical Research Letters* **39**, doi:10.1029/2012gl051106 (2012).

23 Wu, L. X. *et al.* Enhanced warming over the global subtropical western boundary currents. *Nature Climate Change* **2**, 161-166, doi:10.1038/nclimate1353 (2012).

24 McCarthy, G. D., Joyce, T. M. & Josey, S. A. Gulf Stream Variability in the Context of Quasi-Decadal and Multidecadal Atlantic Climate Variability. *Geophysical Research Letters* **45**, 11257-11264, doi:10.1029/2018gl079336 (2018).

25 Wang, Y. L. & Wu, C. R. Discordant multi-decadal trend in the intensity of the Kuroshio along its path during 1993-2013. *Scientific Reports* **8**, doi:10.1038/s41598-018-32843-y (2018).

26 Chen, X. Y. & Tung, K. K. Varying planetary heat sink led to global-warming slowdown and acceleration. *Science* **345**, 897-903, doi:10.1126/science.1254937 (2014).

27 Liu, W., Xie, S. P. & Lu, J. Tracking ocean heat uptake during the surface warming hiatus. *Nature Communications* **7**, 9, doi:10.1038/ncomms10926 (2016).

28 He, C. F., Liu, Z. Y. & Hu, A. X. The transient response of atmospheric and oceanic heat transports to anthropogenic warming. *Nature Climate Change* **9**, 222-+, doi:10.1038/s41558-018-0387-3 (2019).

29 Armour, K. C., Marshall, J., Scott, J. R., Donohoe, A. & Newsom, E. R. Southern Ocean warming delayed by circumpolar upwelling and equatorward transport. *Nature Geoscience* **9**, 549-+, doi:10.1038/ngeo2731 (2016).

30 Mantua, N. J., Hare, S. R., Zhang, Y., Wallace, J. M. & Francis, R. C. A Pacific interdecadal climate oscillation with impacts on salmon production. *Bulletin of the American Meteorological Society* **78**, 1069-1079, doi:10.1175/1520-0477(1997)078<1069:apicow>2.0.co;2 (1997).

31 Salinger, M. J., Renwick, J. A. & Mullan, A. B. Interdecadal Pacific Oscillation and South Pacific climate. *International Journal of Climatology* **21**, 1705-1721, doi:10.1002/joc.691 (2001).

32 Merrifield, M. A. & Maltrud, M. E. Regional sea level trends due to a Pacific trade wind intensification. *Geophysical Research Letters* **38**, 5, doi:10.1029/2011gl049576 (2011).

33 Hamlington, B. D. *et al.* An ongoing shift in Pacific Ocean sea level. *Journal of Geophysical Research-Oceans* **121**, 5084-5097, doi:10.1002/2016jc011815 (2016).

34 Roxy, M. K., Ritika, K., Terray, P. & Masson, S. The Curious Case of Indian Ocean Warming. *Journal of Climate* **27**, 8501-8509, doi:10.1175/jcli-d-14-00471.1 (2014).

35 Caesar, L., Rahmstorf, S., Robinson, A., Feulner, G. & Saba, V. Observed fingerprint of a weakening Atlantic Ocean overturning circulation. *Nature* **556**, 191-+, doi:10.1038/s41586-018-0006-5 (2018).

36 Smeed, D. A. *et al.* The North Atlantic Ocean Is in a State of Reduced Overturning. *Geophysical Research Letters* **45**, 1527-1533, doi:10.1002/2017gl076350 (2018).

37 Josey, S. A. *et al.* The Recent Atlantic Cold Anomaly: Causes, Consequences, and Related Phenomena. *Annual Review of Marine Science, Vol 10* **10**, 475-501, doi:10.1146/annurev-marine-121916-063102 (2018).

38 Durack *et al.* Quantifying underestimates of long-term upper-ocean warming. *Nature Climate Change*, **4**, 999-1005, doi:10.1038/NCLIMATE2389 (2014).

39 Durack *et al*. Ocean warming: From the surface to the deep in observations and models. *Oceanography* **31**(2), 41–51, doi:10.5670/oceanog.2018.227 (2018).

Methods and Data

We combine altimeter and in situ ocean temperature data to produce annual maps of upper (0–700 m) ocean heat content anomalies following ref. 18, referring to them as the PMEL maps throughout. This well-validated method uses regional-scale correlations between ocean heat content and sea-surface height anomalies to generate a first-guess map of ocean heat content directly from sea-surface height. (Where values are missing from the altimeter maps, the first-guess map is set to zero.) It then estimates an innovation by objectively mapping the residuals of in situ ocean heat content values relative to the first-guess map, finally adding that innovation map to the first-guess map. We also use annual maps of 0–700 m ocean heat content anomalies produced from in situ temperature data alone from three other research groups: JMA[20], IAP[21], and NCEI[22].

The Ssalto/Duacs global maps of satellite-altimeter derived sea-surface height anomalies used for the PMEL maps were produced and distributed by the Copernicus Marine and Environment Monitoring Service (CMEMS) and downloaded in January 2019. The in situ Argo data used for the PMEL maps (doi:10.17882/42182#61117) were downloaded from the US Argo Global Data Assembly Center in January 2019. The historical in situ temperature data other than Argo used for the PMEL maps were EN3 v2a[40] from the UK Met Office, derived mostly from the World Ocean Database[41] with updated mechanical and expendable bathythermograph (MBT and XBT) bias corrections[42] already applied. While EN3 v2a has been superseded, there is not much change in more recent versions aside from the addition of Argo data, which we download from the primary source. The JMA, IAP, and NCEI maps used are all publicly available at web addresses noted in the Data accessibility section.

While the combined altimeter method used for the PMEL maps is thoughtfully designed and carefully validated[18], agreement between local estimates or the global integrals of the combined map trends and those from in situ-only maps is not assured;

firstly, because the in situ data prior to Argo are sparse[8] and subject to biases[7], but also because the altimeter sea-surface height values are not a perfect proxy for 0–700 m ocean heat content. After all, sea level also includes a large component from addition of mass from land ice, changes in temperature below 700 m, as well as contributions from changing salinity. The full-depth ocean thermal expansion is estimated to account for 42% of the sea level trend over that time period[2], and the 0–700 m contribution is only a portion of that, albeit a large portion.

For all four set of maps (PMEL, JMA, NCEI, and IAP) we use annual maps at half-year intervals (e.g., 50% overlapping) of ocean heat content anomaly centered on the mid-year (July 2) and the turn of the year (January 1) from July 1993 (or July 1968) through July 2019. The combined method takes advantage of the near-global coverage of sea-surface height anomalies that started in 1993 to allow well constrained global maps of upper ocean heat content anomalies even prior to Argo first reaching sparse global coverage around 2005. Without these first guesses, prior to the advent of near-global Argo coverage in the mid-2000s, large data-sparse areas of the PMEL maps south of ~30°S would be relatively featureless with near-zero (climatological) values[8]. Maps are generated over the entire ocean surface area, which is 361×10^{12} m^2. For the in situ maps for other research groups, the area mapped varies slightly, and is not quite global for some.

To account for the varying instrument types and take the best advantage of their typical depths of maximum measurements[7], the PMEL analysis is done in six carefully chosen depth layers (0–40 m, 40–90 m, 90–190 m, 190–290 m, 290–450 m, and 450–700 m) following ref. 8. The use of depth layers allows use of the full vertical resolution of the in situ temperature profiles. Our aim in using these specific layer depths is to maximize the number of profiles spanning each layer.

The annual PMEL maps, because they incorporate information from individual in situ profiles as well as spatially detailed maps of sea-surface height from altimeter data, resolve (or at least permit) eddy scales[19]. However, the signatures of eddies and other mesoscale variability are noise for our purposes. Hence, we suppress them by filtering each annual map with a 2-dimensional Hanning filter that has half-maxima at 6° longitude and 3° latitude length scales prior to analysis. Prior to smoothing, we linearly interpolate spatially to fill gaps in the maps, allowing the subsequent smoothed fields to extend to ocean boundaries, hence not reducing the analyzed areas at the edges of mapped regions by smoothing. While the results are relatively insensitive to the application of the smoothing step, or variations in the smoothing length scales, the spatial patterns revealed in our analyses are slightly clearer visually and slightly more robust statistically when using the smoothed fields instead of the unsmoothed fields. The results from the smoothed maps are also more similar to the in situ maps made by other research groups, which generally employ larger mapping scales than the PMEL maps because in situ data do not usually resolve eddy scales. Hence, we proceed with the smoothed PMEL maps.

After smoothing, we mask each depth layer using ETOPO2 bathymetry[43] smoothed with a 0.5° lat. × 0.5° long. half-width Hanning filter. We weight the mask using the fraction of the layer present when the smoothed bottom depth at a gridpoint is shallower than the bottom of a layer but deeper than the top of that layer. We then add the masked maps for all layers to make a single 0–700 m layer for analysis.

After smoothing, masking, and summing the layers, we then fit local linear regressions to the resulting fields at each location over time periods ranging from 5 to 27 years (for 1993–2019) for the combined maps. We perform an identical analysis to the in situ-only based maps from the other research groups, and add analysis for 5 to 52 years (for 1968–2019) for those maps, which extend back further in time than 1993.

All analyses use the residuals of the simple least-squares linear fits to find standard errors of the slopes in the regular fashion[44]. We also take into account the effective degrees of freedom for serial correlation in those residuals by using twice the integral of the lagged autocorrelation as an estimate of the decorrelation time scale[45]. We express all estimate uncertainties as 90% two-tailed (5–95%) confidence intervals, assuming Student's t-distribution. While many different choices of confidence intervals could be made, 90% two-tailed (5–95%) confidence intervals are also used in the Fifth Assessment Report of Working Group One to the IPCC[1] and for ocean heat content analyses in annual State of the Climate reports[19]. The uncertainties increase with trend length as the degrees of freedom decrease until reaching about two thirds to the quarters of the record length (Fig. 3). For the longer trend lengths the uncertainties decrease, probably because even the application of Student's t-distribution does not quite make up for the lack of independence in those records.

Data availability

The Ssalto/Duacs global maps of satellite-altimeter derived sea-surface height anomalies used for the PMEL maps were downloaded in January 2019 and can be accessed at https://www.aviso.altimetry.fr/en/data/products/sea-surface-height-products/global.html. The in situ Argo data used for the PMEL maps (doi:10.17882/42182#61117) were downloaded from the US Argo Global Data Assembly Center in January 2019 and can be accessed at https://www.usgodae.org//argo/argo.html. The historical in situ temperature data other than Argo used for the PMEL maps were EN3 v2a from www.metoffice.gov.uk/hadobs. This version has been superseded, but historical non-Argo data in later versions are very similar. The ocean heat content maps from JMA can be accessed at https://www.data.jma.go.jp/gmd/kaiyou/english/ohc/ohc_global_en.html, those from IAP at http://159.226.119.60/cheng/, and those from NCEI at https://www.nodc.noaa.gov/OC5/3M_HEAT_CONTENT/.

Acknowledgements

G.C.J. and J.M.L. are supported by the Global Ocean Monitoring and Observing program, National Oceanic and Atmospheric Administration (NOAA), U.S. Department of Commerce and NOAA Research. The Argo data used here were collected and made freely available by the International Argo Program and the national programs that contribute to it (http://www.argo.ucsd.edu, http://argo.jcommops.org). The Argo Program is part of the Global Ocean Observing System. The Ssalto/Duacs global sea level anomaly maps used here were produced and distributed by the Copernicus Marine and Environment Monitoring Service. We thank two anonymous reviewers and chief editor Dr. Bronwyn Wake for their helpful comments and suggestions. The scientific results and conclusions, as well as any views or opinions expressed herein, are those of the authors and do not necessarily reflect the views of NOAA or the Department of Commerce. PMEL Contribution number 4968.

Author Information

Affiliations

NOAA/Pacific Marine Environmental Laboratory, Seattle WA 98115, USA

Gregory C. Johnson and John M. Lyman

Joint Institute for Marine and Atmospheric Research, University of Hawai'i at Manoa, Honolulu HI 96822, USA

John M. Lyman

Contributions

G.C.J and J.M.L designed the study. J.M.L. made the calculations and analyzed the trends. G.C.J. wrote the manuscript. Both authors contributed to interpreting the results and improving the manuscript

Corresponding Author

Correspondence to Gregory C. Johnson at gregory.c.johnson@noaa.gov

Ethics Declarations

Competing interests

The authors declare no competing interests.

Methods references

40 Ingleby, B. & Huddleston, M. Quality control of ocean temperature and salinity profiles - Historical and real-time data. *Journal of Marine Systems* **65**, 158-175, doi:10.1016/j.jmarsys.2005.11.019 (2007).

41 Locarnini, R. A. *et al. World Ocean Atlas 2009, Volume 1: Temperature* . 184 (2010).

42 Ishii, M. & Kimoto, M. Reevaluation of historical ocean heat content variations with time-varying XBT and MBT depth bias corrections. *Journal of Oceanography* **65**, 287-299, doi:10.1007/s10872-009-0027-7 (2009).

43 Smith, W. H. F. & Sandwell, D. T. Global sea floor topography from satellite altimetry and ship depth soundings. *Science* **277**, 1956-1962, doi:10.1126/science.277.5334.1956 (1997).

44 Wunsch, C. *The Ocean Circulation Inverse Problem.,* (Cambridge University Press, 1996).

45 von Storch, H. & Zwiers, F. W. *Statistical Analysis in Climate Research*. (Cambridge University Press, 1999).

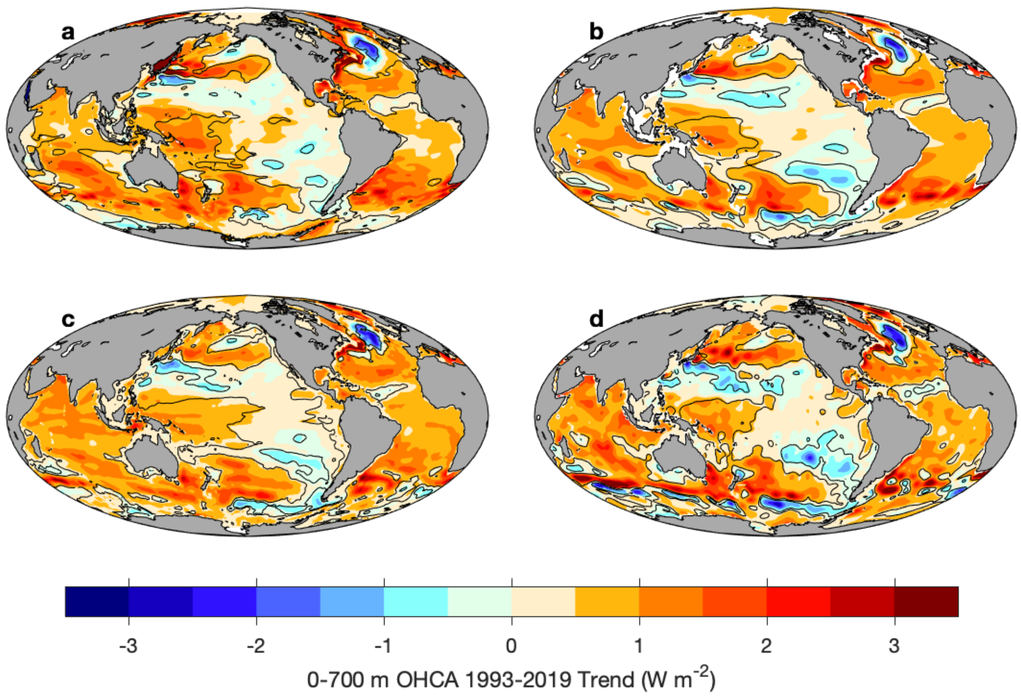

Fig. 1 | Upper (0–700 m) ocean heat content anomaly (OHCA) linear trends for 1993–2019. For annual estimates of (a) the PMEL combined maps, and the in situ-only maps of (b) JMA, (c) IAP, and (d) NCEI. Values are in W m^{-2} (colorbar) applying 90% two-tailed (5–95%) confidence limits to outline areas with trends that are statistically significantly different from zero (black contours).

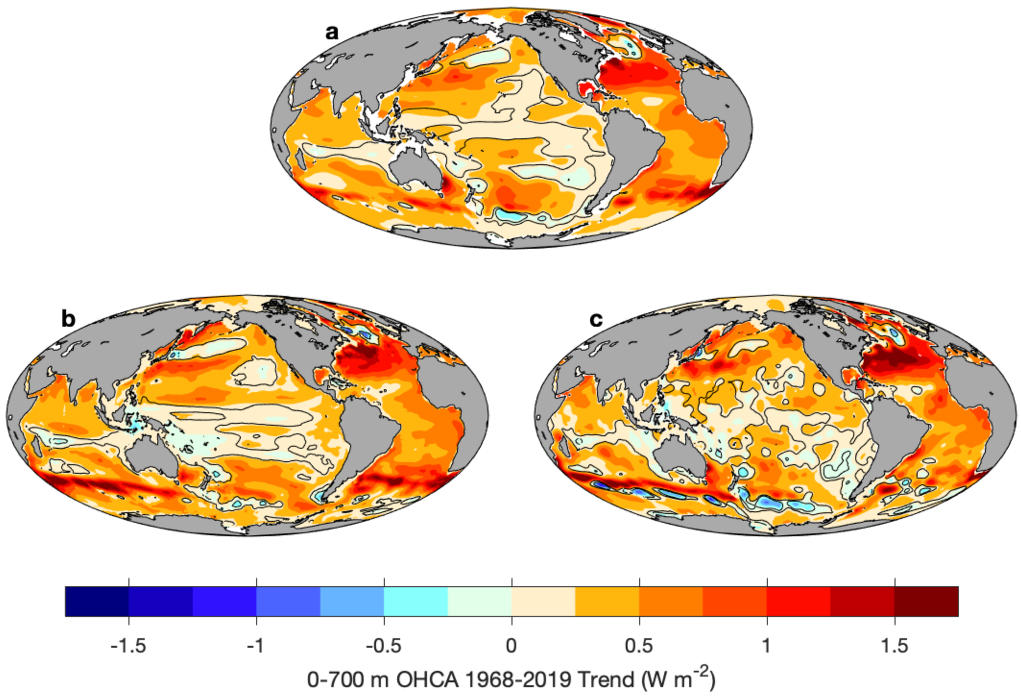

Fig. 2 | Upper (0–700 m) ocean heat content anomaly (OHCA) linear trends for 1968–2019. For annual estimates using the in situ-only maps of (a) JMA, (b) IAP, and (c) NCEI. Values are in W m^{-2} (colorbar) applying 90% two-tailed (5–95%) confidence limits to outline areas with trends that are statistically significantly different from zero (black contours). The scale is half that of Fig. 1.

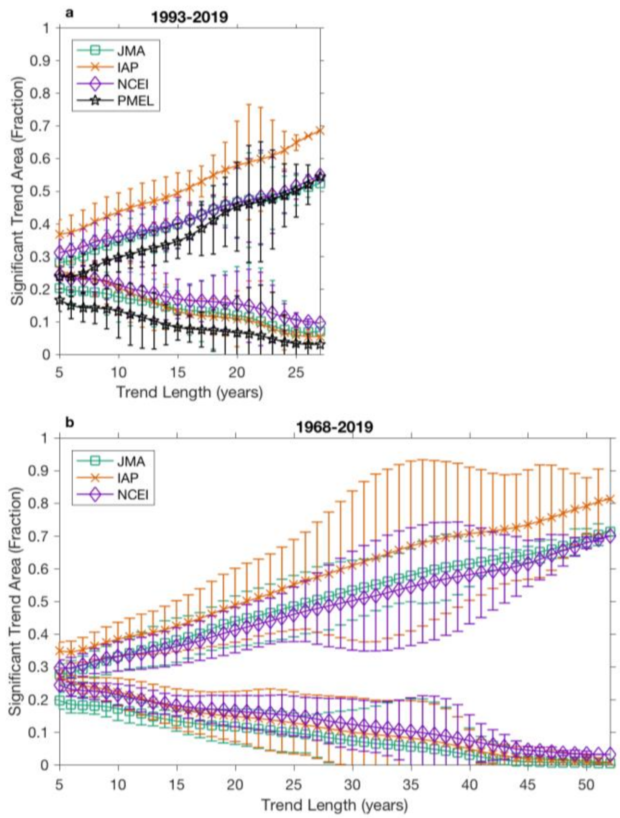

Fig. 3 | Mean fractions of the global ocean surface area with trends of upper (0–700 m) ocean heat content that are statistically significantly different from zero. Annual maps from four different research groups are used for (a) 1993–2019 and (b) 1968–2019. Areas of statistically significant positive trends increase with increasing trend length, and areas of statistically significant negative trends decrease with increasing trend length. Mean and uncertainties are estimated using all possible contiguous periods from 5-year (left side, 43 estimates) to 27-year (a, right side, only one estimate) or 52-year (b, right side, only one estimate) trend lengths. Error bars show 90% two-tailed confidence limits using the variance of the estimates and Student’s t-distribution, estimating the degrees of freedom as the record length (27 or 52 years) divided by the trend length (5 to 27 years or 52 years). Since there is only one realization for the record length trends, their uncertainties are not estimated.

Table 1 | Fractional area of statistically significant positive and negative trends for 0–700 m ocean heat content anomalies. Annual maps from four different research groups are used, with two different record lengths (1993–2019 and 1968–2019) shown.

Product	Time Period	Significantly Positive Trend	Significantly Negative Trend
PMEL	1993-2019	56%	3%
JMA	1993-2019	58%	8%
IAP	1993-2019	68%	5%
NCEI	1993-2019	57%	10%
JMA	1968-2018	79%	1%
IAP	1968-2018	80%	1%
NCEI	1968-2019	72%	3%

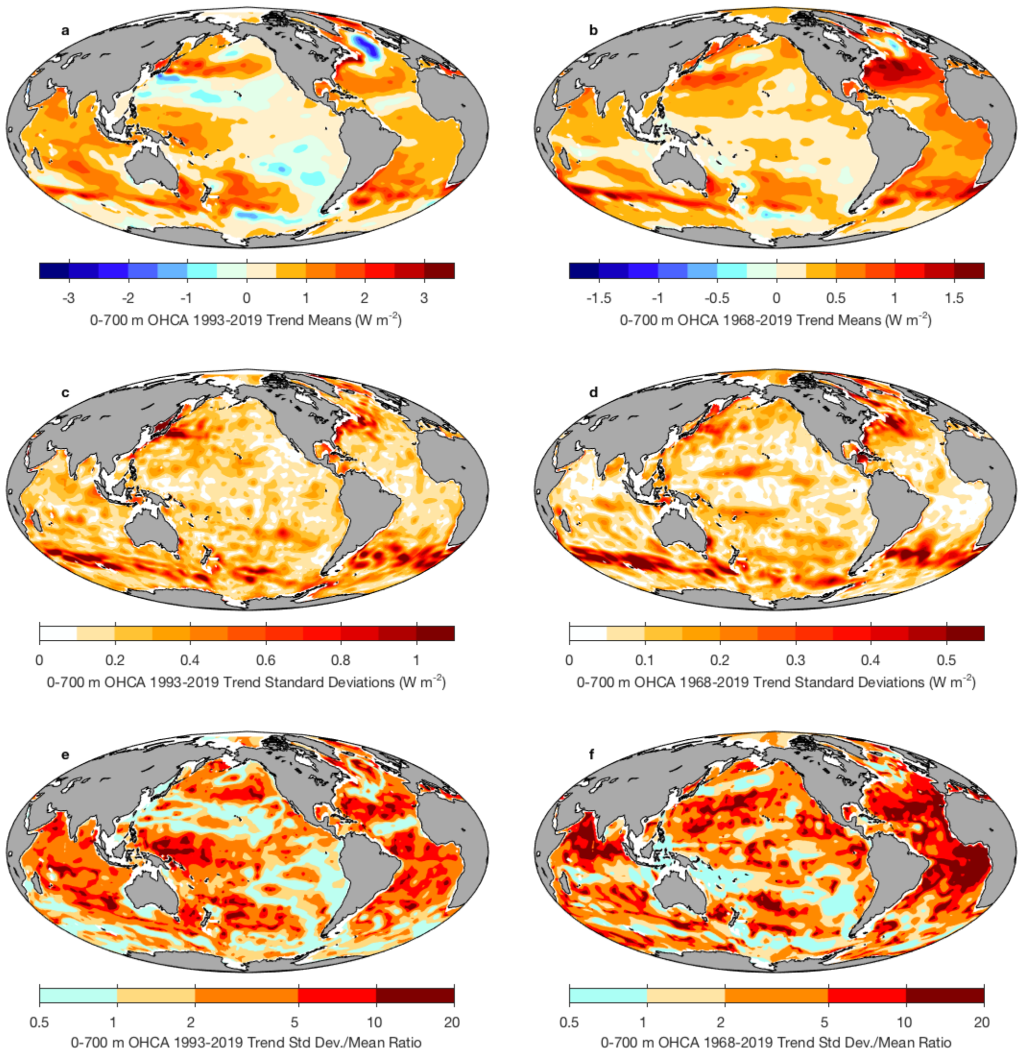

Extended Data Fig. 1: Means, standard deviations, and ratios of their magnitudes for the different 0–700 m ocean heat content trend estimates used. Means of trends for (a) 1993–2019 are contoured over twice the range used for (b) 1968–2019. Similarly, the standard deviations for (c) 1993–2019 trends are contoured over twice the range used for (d) 1968–2019. The ratio of the mean trend magnitudes to their standard deviations are contoured on the same scale for (e) 1993–2019 and (f) 1968–2019.